CMA
CONSTRUCTIVE MATHEMATICAL ANALYSIS

Research Article

A comparison among a fuzzy algorithm for image rescaling with other methods of digital image processing

Danilo Costarelli and Anna Rita Sambucini*

ABSTRACT. The aim of this paper is to compare the fuzzy-type algorithm for image rescaling introduced by Jurio et al., 2011, quoted in the list of references, with some other existing algorithms such as the classical bicubic algorithm and the sampling Kantorovich (SK) one. Note that the SK algorithm is a recent tool for image rescaling and enhancement that has been revealed to be useful in several applications to real world problems, while the bicubic algorithm is widely known in the literature. A comparison among the abovementioned algorithms (all implemented in the MatLab programming language) was performed in terms of suitable similarity indices such as the Peak-Signal-to-Noise-Ratio (PSNR) and the likelihood index S.

Keywords: *Fuzzy-type algorithm, SK algorithm, bicubic algorithm, PSNR, S index, image magnification.*

2020 *Mathematics Subject Classification:* 94A08, 68U10, 41A35, 41A30, 03E72.

1. INTRODUCTION

Images are indispensable tools in concrete life, as well as in various fields of research and they have a concrete impact on daily life. The most common scientific applications of image processing are in medicine, in which some instrumental tests such as CT and MRI, are helpful for the diagnosis of various diseases, remote sensing, in which the use of satellite images allows the study of phenomena (climatic, tectonic, etc) linked to natural events; astronomy, biology and many other fields. In real world applications digital images are essential tools for studying concrete problems since they provide visual and numerical representations of an observation or a measurement. Namely, they constitute a synthesis of information concerning one or more characteristics of the problem under consideration. The acquisition of a digital image from a camera or a diagnostic device is a physical process that allows the conversion of measured data into two or three dimensional discrete signals/images. During this phase, the acquisition tools, which are obviously endowed with their own sensitivity and by their own procedure of data conversion, allow the reconstruction of a digital image that is obviously characterized by a natural degree of approximation and therefore of uncertainty, i.e., it is not always possible to establish the gray levels of a region of pixels perfectly or to precisely detect geometric shapes characteristics, such as edges of particular interest.

These facts can be translated into the construction of a matrix of pixels in which the value of each element represents a "good approximation" of the real gray level (luminance) in the gray scale. When situations of this type are present, it is possible to use fuzzy set theory to represent and elaborate vague and imprecise concepts and apply a fuzzy algorithm for digital

image processing, as in, for example [16, 25, 35, 42, 45]. Moreover, we also know that fuzzy theory is a fundamental tool for several topics, such as probability (see, e.g., [6, 36, 49]) and many others, hence it is not surprising to find a close connection between digital images and their processing. Recently multifunctions have also been applied for convergence results in this setting see also [37–39].

On the other hand, it is also known that any image is a multivariate discontinuous signal, where the possibility of visualizing the contours and edges in the figures is due to the presence of meaningful jumps of gray levels in the grayscale; this is the motivation why Signal Theory has been successfully applied to process digital images. Indeed, in the last ten years, several models for concrete applications in the field of medicine and engineering have been developed thanks to the use of the SK algorithm (e.g., [24, 32, 47]). The main purpose of the SK algorithm is to rescale images, by acting as low-pass filter and hence contrasting the appearance of noise. The SK algorithm is the numerically optimized implementation of the sampling Kantorovich operators (from which the acronym SK), widely studied in Approximation Theory, since it is very suitable for reconstructing non-necessarily continuous signals (hence images, see [31, 33]).

The aim of this paper is to compare the fuzzy-type algorithm introduced in [42] with the classical bicubic interpolation method, widely used in the literature e.g., [46] and the above described SK algorithm. The above algorithms were implemented in the MatLab programming language, and comparisons were performed by means of several numerical tests performed on a suitable dataset of images of different types. To quantitatively evaluate the results, we introduced two similarity indices known in the literature. We considered the Peak-Signal-to-Noise-Ratio (PSNR) [50], and the likelihood index S considered in [17]. Finally, a comparison in terms of CPU time employed by the three considered algorithms was also carried out for the best approximations.

2. The Interval valued Fuzzy point of view

A grayscale digital image of dimensions $n \times m$ (i.e., with n rows and m columns) is a matrix Q of dimensions $n \times m$, where the element of position (i, j) in the matrix, denoted by $q_{i,j}$, represents the intensity of the pixel in the gray scale (luminance). We observe that it is not restrictive to work only with grayscale images, since operating on a color image is similar to doing so on 3 grayscale images. For colour images three matrices are used which, for each pixel, assume integer values in the range $[0, 255]$ with respect to the red, green and blue colours (RGB channels, see, for example, [41]).

The luminance values $q_{i,j}$ at point (i, j) are normalized to obtain values in the range $[0, 1]$. To simplify the notation, we will always indicate them with the same symbol.
In [42], Jurio, Paternain, Lopez-Molina, Bustince, Mesiar and Beliakov proposed a model associated to a grayscale image and an interval valued fuzzy set to construct a magnification algorithm that considers the luminance values in a neighbourhood of each pixel of the image.

The type of operator they use is of spatial type, namely, to determine the value of the destination pixels, not only the value of the pixel in the original image but also the value of some pixels close to it (in a neighbourhood of it) will be considered.

The key idea of this rescaling algorithm (proposed by Jurio et al.) is to associate an interval membership to each pixel. The parameter δ is fixed a priori; when δ increases the length of the interval increases, so more values of the intensities of the pixels close to the assigned intensity are considered. In this way, a new block is constructed for each pixel of the image, and the central pixel of the block maintains the luminance of the original pixel. To fill the rest of the pixels in the newly generated block, the relationship between the luminance of the pixel in the original image and that of the pixels "near" to the pixel was used.

To define the interval-valued membership of $q_{i,j}$, let $L([0,1])$ be the family of all closed intervals in $[0,1]$, namely

$$L([0,1]) := \{ \mathbf{x} = [x_\star, x^\star] : (x_\star, x^\star) \in [0,1]^2 \ \& \ x_\star \leq x^\star \},$$

with the following partial order relation: $\mathbf{x} \leq_L \mathbf{y}$ if $x_\star \leq y_\star$ and $x^\star \leq y^\star$ (this is a lattice order between closed intervals; see, for example, [42]). For every closed interval $\mathbf{x} := [x_\star, x^\star]$ in $L([0,1])$, let $W(\mathbf{x}) := x^\star - x_\star$ be its length.

Therefore, an interval-valued membership of $q_{i,j}$ is an interval valued fuzzy set (IVFS for short) A, namely a map $A : Q \to L([0,1])$ that assigns to each position (i,j) an interval $\mathbf{x}^{i,j}$ (see next formula (2.4)).

Let $\alpha \in [0,1]$ be fixed, and let $K_\alpha : L[0,1] \to [0,1]$ be a function, given in [7, 14, 15, 34], such that for every $\mathbf{x} \in L([0,1])$ and $\alpha \in [0,1]$,

k.1): $K_0(\mathbf{x}) = x_\star$, $\quad K_1(\mathbf{x}) = x^\star$, $\quad K_\alpha(\mathbf{x}) = x_\star$ if $x_\star = x^\star$;
k.2): for every $\alpha \in [0,1]$ $K_\alpha(\mathbf{x}) = K_0(\mathbf{x}) + \alpha(K_1(\mathbf{x}) - K_0(\mathbf{x}))$;
k.3): if $\mathbf{x} \leq_L \mathbf{y}$, $\mathbf{x}, \mathbf{y} \in L([0,1])$ then $K_\alpha(\mathbf{x}) \leq K_\alpha(\mathbf{y})$ for every $\alpha \in [0,1]$;
k.4): $\alpha \leq \beta$ if and only if $K_\alpha(\mathbf{x}) \leq K_\beta(\mathbf{x})$ for every $\mathbf{x} \in L([0,1])$.

The operator K_α is known in the literature as Atanassov's operator.

Using K_α, it is possible to associate an interval-valued fuzzy set with a fuzzy set in the following way:

$$(2.1) \qquad K_\alpha(\mathbf{x}) = K_\alpha([x_\star, x^\star]) = x_\star + \alpha(x^\star - x_\star) = x_\star + \alpha W(\mathbf{x}).$$

In practice, Atanassov's operator of order α is a convex combination of the end points of its argument $\mathbf{x} = [x_\star, x^\star] \in L[0,1]$.

Remark 2.1. There are other possible constructions of the multifunction K_α, and the choice of the previous operator is motivated by the length of the interval being fundamental in the magnification process given in [42], since the length of each interval membership is fixed a priori.

2.1. **Interval-valued fuzzy model.** We provide a description of the algorithm based on the above interval-valued fuzzy model. For the sake of brevity, we often refer to such an algorithm with the term "fuzzy-type algorithm".

As previously mentioned let Q be an $n \times m$ matrix associated with a grayscale image. Let $\delta \in [0,1]$ and $p \in \mathbb{N}$. For every $i \in \{1, 2, \ldots, m\}$ and $j \in \{1, 2, \ldots, n\}$ let $q_{i,j}$ be the value of element (i,j) in Q.

For every $i \in \{1, 2, \ldots, m\}$ and $j \in \{1, 2, \ldots, n\}$, let $V_{i,j} = (v_{k,l}^{(i,j)})_{k,l}$ a $(2p+1) \times (2p+1)$ square matrix (also named block) centered at the position (i,j), namely the value $v_{p+1,p+1}^{(i,j)}$ coincides with $q_{i,j}$, and is used to obtain the magnification of Q.

Let $v_{k,l}^{(i,j)}$ be the elements of $V_{i,j}$ with $k, l \in \{1, 2, \ldots, 2p+1\}$;

$$(2.2) \qquad v_{k,l}^{(i,j)} = \begin{cases} q_{i-p+k-1, j-p+l-1} & \text{if } i-p+k-1 \in \{1, 2, \ldots, n\}, \\ & \qquad\quad j-p+l-1 \in \{1, 2, \ldots, m\} \\ 0 & \text{elsewhere.} \end{cases}$$

This means that if there are positions (k,l) in $V_{i,j}$ that are not covered by elements of Q (i.e., if in the superposition of the block $V_{i,j}$ with the matrix Q there are some elements that do not belong to Q), the corresponding values in the matrix $V_{i,j}$ are set to zero.

To define a neighborhood of $q_{i,j}$, the oscillation $\omega_{i,j}$ of the values in $V_{i,j}$ is calculated without

considering the possible presence of the added null values in the block , namely,

$$\omega_{i,j} = \left(\max_{\substack{i-p+k-1 \in \{1,2,\ldots,n\}, \\ j-p+l-1 \in \{1,2,\ldots,m\}}} q_{i-p+k-1,j-p+l-1} \right)$$

(2.3)
$$- \left(\min_{\substack{i-p+k-1 \in \{1,2,\ldots,n\}, \\ j-p+l-1 \in \{1,2,\ldots,m\}}} q_{i-p+k-1,j-p+l-1} \right),$$

and a closed interval $F(q_{i,j}, \omega_{i,j}, \delta) \in L([0,1])$ is assigned to each $q_{i,j}$, as follows:

(2.4)
$$F(q_{i,j}, \omega_{i,j}, \delta) = [q_{i,j}(1 - \delta\omega_{i,j}), q_{i,j}(1 - \delta\omega_{i,j}) + \delta\omega_{i,j}].$$

Therefore the intensities of the pixels in this generated block provide information for obtaining the length of the interval-valued membership built using F. For this interval-valued membership in $L([0,1])$, Atanassov's operator (2.1) is applied to construct a new square matrix

$$V'_{i,j} = (v'_{k,l})_{k,l}, \qquad k,l \in \{1,2,\ldots,2p+1\},$$

whose elements are obtained in the following way:

$$\begin{aligned}
v'_{k,l} :=& K_{v^{(i,j)}_{k,l}}(F(q_{i,j}, \omega_{i,j}, \delta)) \\
=& K_{v^{(i,j)}_{k,l}}([q_{i,j}(1 - \delta\omega_{i,j}), q_{i,j}(1 - \delta\omega_{i,j}) + \delta\omega_{i,j}]) \\
=& v^{(i,j)}_{k,l} \cdot \left(q_{i,j}(1 - \delta\omega_{i,j}) + \delta\omega_{i,j} \right) + (1 - v^{(i,j)}_{k,l}) \cdot q_{i,j}(1 - \delta\omega_{i,j}) \\
=& v^{(i,j)}_{k,l} \delta\omega_{i,j} + q_{i,j}(1 - \delta\omega_{i,j}).
\end{aligned}$$

Finally, in the new rescaled image, each element $q_{i,j}$ is replaced by the new block $V'_{i,j}$. We can observe that if $\delta = 0$ the information on the boundary is lost since $F(q_{i,j}, \omega_{i,j}, \delta) = q_{i,j}$.

3. OTHER METHODS

To evaluate the performance of the considered fuzzy-type algorithm, in the numerical tests performed in Section 5, we consider the rescaling of a given dataset of images with the well-known bicubic method, which is very classical in digital image processing, and is already implemented in several software and dedicated commands are available in most used programming languages) and we compare it with the SK algorithm which will be recalled in the next subsection.

3.1. **The Sampling Kantorovich algorithm for image rescaling.** An algorithm that has been widely applied in the field of image rescaling is known for its name, the sampling Kantorovich (SK) algorithm; see, e.g., [8, 47]. The above tool arises as an optimized implementation of a family of sampling-type operators, that is, the multivariate SK operators, defined through the following formula:

(3.5)
$$(S_w f)(\vec{x}) := \sum_{\vec{k} \in \mathbb{Z}^2} \chi(w\vec{x} - \vec{k}) \left[w^2 \int_{R^w_{\vec{k}}} f(\vec{u}) \, d\vec{u} \right], \qquad \vec{x} \in \mathbb{R}^2, \quad w > 0,$$

where $f : \mathbb{R}^2 \to \mathbb{R}$ is a locally integrable function (signal/image) such that the above series is convergent for every $\vec{x} \in \mathbb{R}^2$, and

$$R^w_{\vec{k}} := \left[\frac{k_1}{w}, \frac{k_1 + 1}{w} \right] \times \left[\frac{k_2}{w}, \frac{k_2 + 1}{w} \right],$$

are the squares in which we consider the averaged values of the sampled signal f (see for example [20, 21]).

S_w, $w > 0$, are approximation operators that can pointwise reconstruct continuous and bounded signals, and to uniformly reconstruct signals that are uniformly continuous and bounded, as $w \to +\infty$. Moreover, the S_w operator can also be used to reconstruct not-necessarily continuous signals, e.g., signals belonging to the L^p-spaces, $1 \leq p < +\infty$ ([2–5, 8–10, 12, 13, 19, 29, 30, 33, 40, 43, 44, 52]). The function $\chi : \mathbb{R}^2 \to \mathbb{R}$, given in (3.5), is called a *kernel* and it satisfies the following suitable assumptions, very typical in this situation, which are the usual conditions assumed by discrete approximate identities (for more details, see, e.g., [1]). Below, we present a list of functions that can be used as kernels in the formula recalled in (3.5).

First, we recall the definition of the one-dimensional central B-spline of order N (for example see [18]):

$$(3.6) \qquad \beta^N(x) \ := \ \frac{1}{(N-1)!} \sum_{i=0}^{N} (-1)^i \binom{N}{i} \left(\frac{N}{2} + x - i \right)_+^{N-1}, \qquad x \in \mathbb{R}.$$

The corresponding bivariate version of the central B-spline of order N is given by:

$$(3.7) \qquad \mathcal{B}_2^N(\vec{x}) \ := \ \prod_{i=1}^{2} \beta^N(x_i), \qquad \vec{x} = (x_1, x_2) \in \mathbb{R}^2.$$

Other important kernels are given by the so-called Jackson type kernels of order N, defined in the univariate case by:

$$(3.8) \qquad J_N(x) \ := \ c_N \operatorname{sinc}^{2N} \left(\frac{x}{2N\pi} \right), \qquad x \in \mathbb{R},$$

with $N \in \mathbb{N}$ and c_N is a nonzero normalization coefficient, given by:

$$c_N \ := \ \left[\int_{\mathbb{R}} \operatorname{sinc}^{2N} \left(\frac{u}{2N\pi} \right) du \right]^{-1}.$$

For the sake of completeness, we recall that the well-known $sinc$-function is defined as $\sin(\pi x)/\pi x$, if $x \neq 0$, and 1 if $x = 0$; see e.g., [43, 44]. As in the case of the central B-splines, the bivariate Jackson type kernels of order N are defined by:

$$(3.9) \qquad \mathcal{J}_N^2(\vec{x}) \ := \ \prod_{i=1}^{2} J_N(x_i), \qquad \vec{x} = (x_1, x_2) \in \mathbb{R}^2.$$

In particular, Jackson type kernels have been revealed to be very useful, e.g., for applications in the biomedical field, [47]. For the numerical tests given in this paper, we consider the bivariate Jackson-type kernel with N varying from 2 to 12. This choice will be motivated later. For several examples of kernels, see, e.g., [23, 26–28]; for more details about the SK operators and the corresponding SK algorithm, see e.g., [24], where a pseudo-code is also available. For some applications of the SK algorithm to real world problems involving images, see, e.g., [31, 47].

4. COMPARISONS AND EVALUATION OF THE NUMERICAL RESULTS: LIKELIHOOD INDEX S AND PSNR

To compare the considered algorithms for image rescaling, we use the following indices that are known in the literature. The first tool is the Peak Signal-to-Noise Ratio (PSNR), which is a well known index in the literature and is often used to quantify the rate of similarity between two general signals.

The PSNR is defined as the Mean Square Error (MSE): $MSE = \sum_{i=1}^{N} \sum_{j=1}^{M} \frac{|I(i,j) - I_r(i,j)|^2}{NM}$,

where I is the original image, I_r is the reconstructed version of the original image I, N and M are the dimensions of the images. Therefore the PSNR is generally defined as follows: $PSNR = 10 \cdot \log_{10} \left(\frac{f_{max}^2}{MSE} \right)$, where f_{max} represents the maximum value of the considered pixel's scale. For 8-bit gray scale images $f_{max} = 255$, while for images with pixel values between 0 and 1 (such as those considered in our fuzzy algorithm) $f_{max} = 1$. Hence, the PSNR formula used in this paper is expressed as follows:

$$(4.10) \qquad PSNR = 10 \cdot \log_{10} \left(\frac{1}{MSE} \right).$$

It is clear from the above definition that, the similarity between two images is greater for the highest values of the PSNR.

Furthermore, we use another useful similarity index, called the likelihood index S, which was introduced by Bustince, et al. ([17]), and is defined as follows:

$$(4.11) \qquad S := \frac{1}{N \times M} \sum_{i=1}^{N} \sum_{j=1}^{M} \left[1 - |I(i,j) - I_r(i,j)| \right],$$

where the notations used in (4.11) are the same as those employed in the definition of the PSNR (4.10). It is clear from the above definition that, the parameter S can assume values between 0 and 1, and that for closer images S should be as close as possible to 1.

5. NUMERICAL EXPERIMENTS

In this section, we provide a numerical comparison among the algorithms considered in the previous sections, namely the fuzzy-type algorithm, the classical bicubic and the SK algorithm. Such a comparison will be carried out thanks to the similarity indices previously recalled, i.e., the PSNR and the likelihood index S.

For the numerical tests, we proceed as follows. We first consider a set of original images of a given dimension $N \times M$, which will be used as a reference. Such images will be reduced without interpolation (using the nearest neighbor method [11]) to the dimension $\frac{N}{3} \times \frac{M}{3}$. Finally, the reduced images will be rescaled to the original dimension by using the methods mentioned above. In this way, we dispose of a reference image (the original image), and three reconstructed images generated by the three different methods mentioned above. With respect to the application of the algorithm based on sampling Kantorovich operators, in view of the accurate experimental analysis given in [31], the SK algorithm has been applied using the parameters that have been seen to be the best possible under certain qualitative criteria (for more details see [31] again). More precisely, we consider the bivariate Jackson-type kernel $\mathcal{J}_N^2$ with $N \in \{2, 3, \ldots 12\}$.

Concerning the parameter w in the SK algorithm, we consider the following values: $w = 5, 10, 15, 20$, and 25 only for the baboon image *.

The image dataset (the source files are contained in the repository https://links.uwaterloo.ca/Repository.html or in [22]) is composed of the four different grayscale images shown in Figure 1. There are the classical "baboon" and "boat", which are commonly used in image analysis, and two pictures of a "city" and a "mountain", respectively.

–––––––––––

* Note that, as stated in [31], in the case of the rescaling of images with double dimensions, it is sufficient to choose $w = 15$ when $N = 12$.
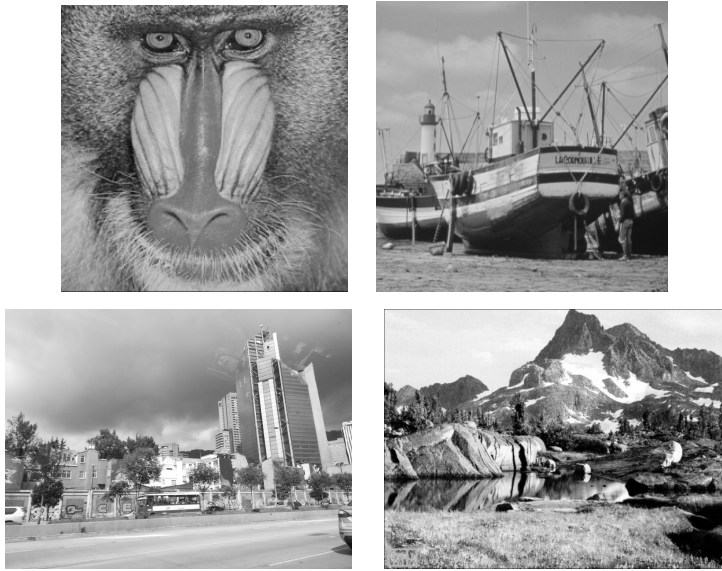
FIGURE 1. Reference images: baboon (255×255 pixel resolution); boat (504×504 pixel resolution); city (675×900 pixel resolution); mountain (450×600 pixel resolution).

The choice of the four images is motivated by the fact that we want to compare images of different sizes, brightness levels and textures. Finally the boat image was also considered in the quoted paper [42], but we do not know if it has the same dimension or resolution. The histograms of the four images show that the distributions of the grayscale of the various images are very different from each other (see Figure 2).
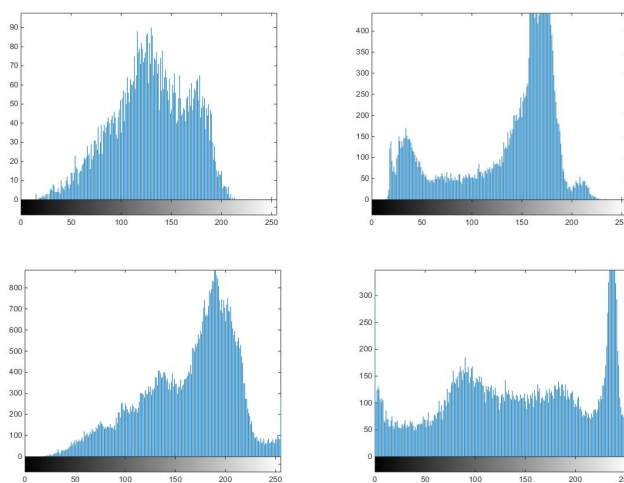
FIGURE 2. Histograms of the original images in the dataset: baboon, boat, city, mountain.

The empirical simulation of the two algorithms is performed on Windows 11 operating system with an Intel Core i7 8th gen. Moreover, all the programs are written and compiled on MATLAB version R2014b.

Concerning the application of the fuzzy-type algorithm, we provide the rescaled images for values of the parameter δ running between 0 and 1, with a step-size equal to 0.01, for each of the images given in Figure 1. The corresponding results of the PSNR and likelihood index S are plotted in Figure 3.
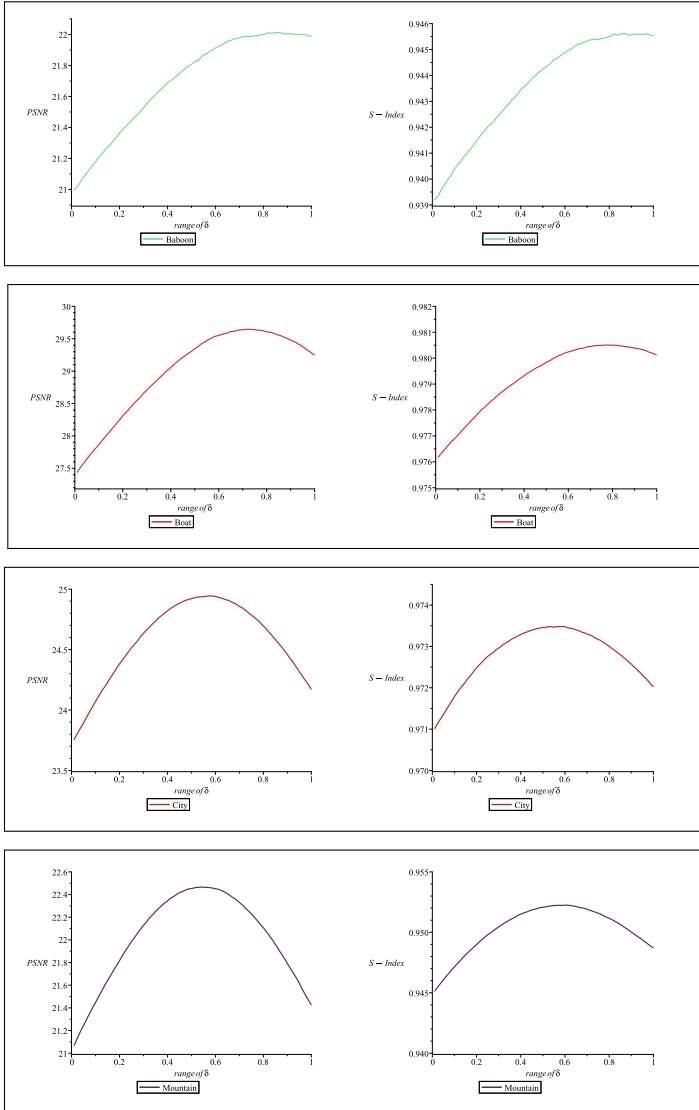
FIGURE 3. The plots of the values of the PSNR and likelihood index S computed for the whole dataset of reconstructed images by the fuzzy-type algorithm when the parameter δ varies from 0 to 1 with step-size of 0.01.

Similarly we rescaled the dataset images using the Sampling Kantorovich algorithm and we examined the values of the similarity indices corresponding to the parameters N and w given in (3.5) and (3.8). The w parameter determines the amount of the sample values that are involved in the reconstruction process, while $2N$ represents the order of decay of the considered kernel function. In particular, we examined the parameter N varying in the set $\{2, 3, \ldots, 12\}$ and the parameter $w \in \{5, 10, 15, 20, 25\}$. Here there are plots of the values of the PSNR and likelihood S indices computed for the reconstructed dataset images with the Sampling Kantorovich algorithm for the considered values of the parameter N of the bivariate Jackson kernel (3.8).
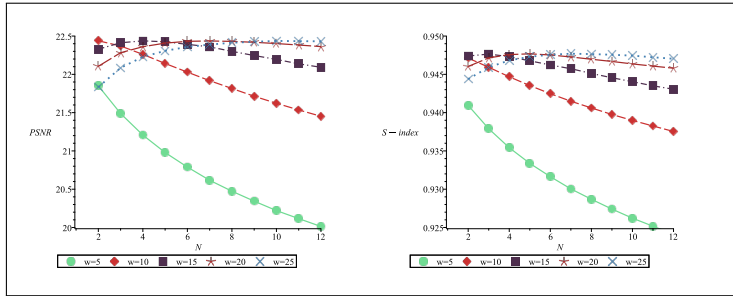
FIGURE 4. The plots of the values of the computed indices for the reconstructed baboon images.
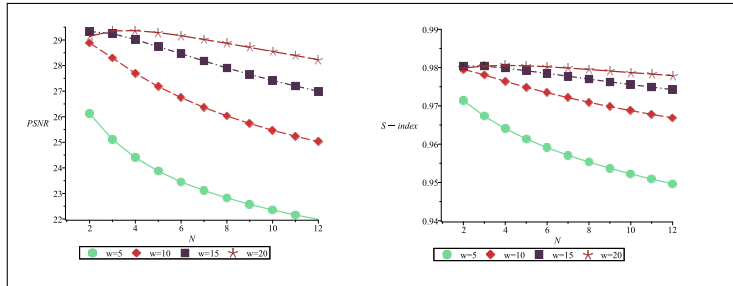
FIGURE 5. The plots of the values of the computed indices for the reconstructed boat images.
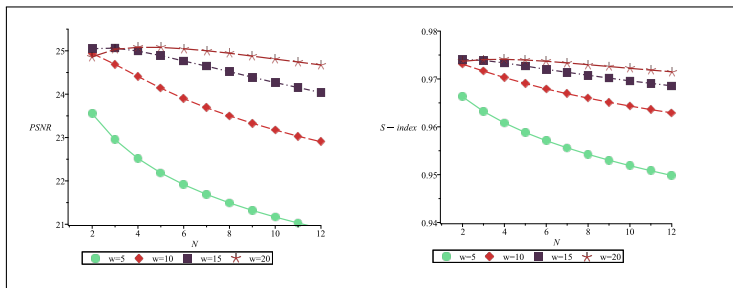
FIGURE 6. The plots of the values of the computed indices for the reconstructed city images.
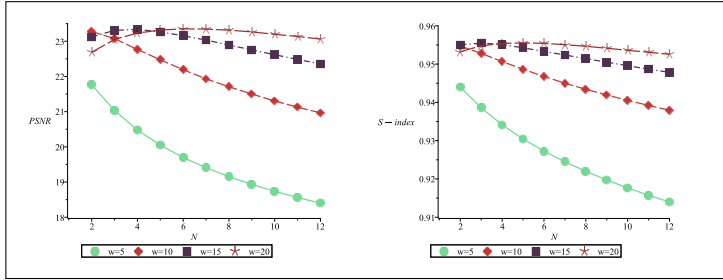
FIGURE 7. The plots of the values of the computed indices for the reconstructed mountain images.

For a more detailed version of these numerical outputs, see the Appendix 6 where all indices are calculated for the SK algorithm.

To provide a more detailed comparison of the numerical results shown in Figures 3, 4, 5, 6 and 7, we also provide additional and useful data in the following tables.

In Table 1, the values of the PSNR are listed and analysed in the case of the fuzzy-type algorithm, together with a comparison with the bicubic method and the SK algorithm. In particular

- in the first column : "$\delta_{Psnr}^{\max}$" denotes the minimum value of the parameter δ for which the maximum PSNR is reached, when the images processed by the fuzzy-type algorithm are considered;
- "PSNR max - Fuzzy" denotes the maximum value of the PSNR reached by implementing the fuzzy-type algorithm for $\delta_{Psnr}^{\max}$;
- "PSNR - bicubic" denotes the values of the PSNR achieved by the image processed by the bicubic algorithm;
- "$(N, w)_{Psnr}^{\max}$" denotes the value of the pair (N, w) for which the best value of the PSNR is reached when the image is processed using the SK algorithm;
- "PSNR - SK" denotes the values of the PSNR achieved by the image processed by the SK algorithm for $(N, w)_{Psnr}^{\max}$.

Note that, in all the above cases the PSNR is computed using the original image of dimension $N \times M$ as the reference image.

TABLE 1. The numerical values of the PSNR.

Image	δ_{PSNR}^{max}	PSNR $\delta_{Psnr}^{\max}$ Fuzzy	PSNR bicubic	$(N, w)_{Psnr}^{\max}$	PSNR $(N, w)_{Psnr}^{\max}$ SK
Baboon	0.86	22.0121	22.2143	(2,10) (see Table 5)	22.43814
Boat	0.72	29.6480	28.0849	(4,20) (see Table 7)	29.3667
City	0.58	24.9440	24.4878	(4,20) (see Table 9)	25.08078
Mountain	0.55	22.4655	21.4886	(6,20) (see Table 11)	23.35247

Moreover, in Table 2, which has the same meaning as in Table 1, the values of the likelihood index S are listed and analysed, for the case of the fuzzy-type, bicubic and SK algorithms.

TABLE 2. The numerical values of the likelihood index S.

Image	$\delta_S^{\max}$	S index $\delta_S^{\max}$ Fuzzy	S index bicubic	$(N,w)_S^{\max}$	S index $(N,w)_S^{\max}$ SK
Baboon	0.86	0.9456	0.9449	(7,25) (see Table 6)	0.947694
Boat	0.78	0.98051	0.9771	(4,20) (see Table 8)	0.980565
City	0.58	0.9735	0.9711	(4,20) (see Table 10)	0.974093
Mountain	0.61	0.9523	0.9455	(5,20) (see Table 12)	0.955541

In Tables 1 and 2, we observe a similar trend in performances with respect to the two indices with the exception of the boat image in which the fuzzy algorithm performs better than the SK at least with respect to the PSNR index and in the baboon image where the best resolutions for the SK algorithm are obtained for $(N,w)_{Psnr}^{\max}$ and $(N,w)_S^{\max}$ which are very distant from each other.

Finally, an analysis concerning the CPU time employed by each of the considered algorithms to process any single image can be performed. The CPU times are listed in Table 3. Since it is not the purpose of the present study to determine all the CPU times, we consider and compare only the times of the best reconstructions. Therefore in Table 3, the values of CPU times are considered for the reconstructed images obtained for $\delta_{Psnr}^{\max}$, $\delta_S^{\max}$, for the fuzzy algorithm and $(N,w)_{Psnr}^{\max}$, $(N,w)_S^{\max}$, for the SK algorithm and quoted in Tables 2 and 3.

TABLE 3. The CPU for the rescaled images of the best approximations for the PSNR and the likelihood index S.

Case n=3	dim image	bicubic	Fuzzy $\delta_{Psnr}^{\max}$	SK $(N,w)_{Psnr}^{\max}$	Fuzzy $\delta_S^{\max}$	SK $(N,w)_S^{\max}$
			The CPU time for the best approximations with respect to PSNR and S indices			
Baboon	255×255	0.054889	2.532010	192.986372	2.532010	5.350619
Boat	504×504	0.091244	0.694429	40.098191	0.585434	40.098191
City	675×900	0.100341	1.137932	192.654707	1.137932	192.654707
Mountain	450×600	0,084561	0.690313	22.639233	0.595628	17.945265

Remark 5.1. Note that as the parameter N increases, the order of decay of the Jackson kernel increase as well and therefore the CPU time of the SK algorithm decreases; however, the similarity indices worsen. The SK algorithm is the most expensive from the point of view of CPU time. If, however, instead of considering its best approximation, we take into account the values of (N,k) so that N is large enough and the SK algorithm performs better than the fuzzy one, we can strongly reduce the CPU time. For example if we consider the reconstructed image of Baboon with $N = 12$ and $w = 15$, we need $2.857455s$ and we obtain, accordingly to Table 5, a better result with respect to the fuzzy algorithm in a much shorter time than $(N,w)_{Psnr}^{\max}$. However if we look at Tables 5-12, in the Appendix, we can see that, except for the boat, the

values of the PSNR or S-index for the SK algorithm are better than those of the fuzzy algorithm when N is quite large, so, in this case, the CPU times of the SK algorithm decrease, continuing to achieve better performances.

For the sake of completeness, we also considered the case of the application of the above-mentioned rescaling algorithms by a resize factor $R = (2k + 1)$, $k = 2, 3$. In practice, we repeated the above experiments reducing the considered original images to have dimension of $\frac{N}{2k+1} \times \frac{M}{2k+1}$, $k = 2, 3$. Consequently, by the above methods, they have been processed in order to reobtain images scaled to the original dimension. Due to the compatibility between the amplitude of the scale factor and the dimensions of the original images, in this case we considered the images "baboon" and "mountain" for $k = 2$ and "boat" for $k = 3$, for the application of the SK algorithm. The corresponding numerical results of this case are presented in Figures 8 and 9. Additionally here, the fuzzy-type algorithm is applied for every δ between 0 and 1, with the same step-size of 0.01.
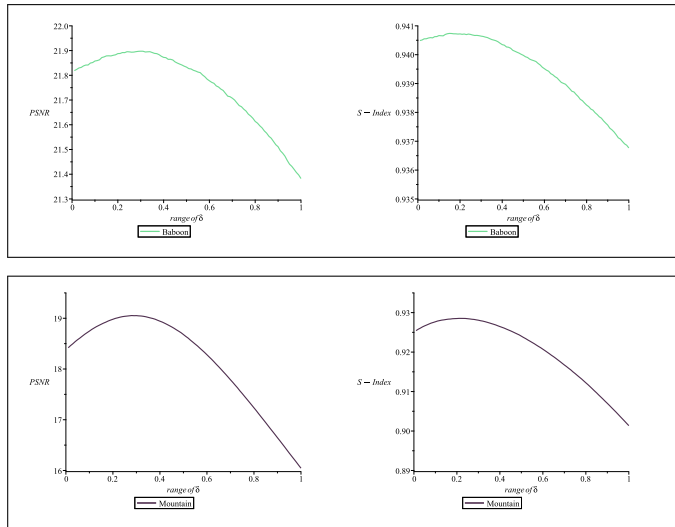
FIGURE 8. $R = 5$: the plots of the values of the PSNR and likelihood index S computed for of the reconstructed images of baboon and mountain with the fuzzy-type algorithm when the parameter δ varies from 0 to 1 with step-size of 0.01.
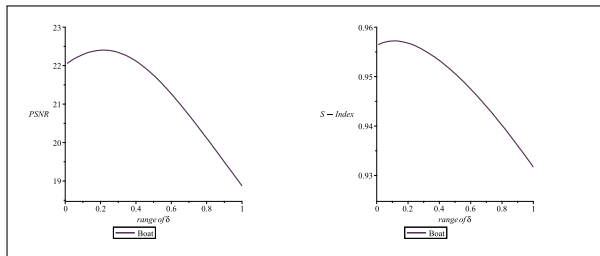
FIGURE 9. $R = 7$: the plots of the values of the PSNR and likelihood index S computed for the reconstructed images of boat with the fuzzy-type algorithm when the parameter δ varies from 0 to 1 with step-size of 0.01.

Remark 5.2. The performances of the fuzzy-type algorithm are dependent on the value of the parameter δ. In all the considered cases, it seems that the curves of the PSNR and S index plots are both concave and achieve a maximum approximatively in the middle zone of the interval $[0,1]$, if we consider the experiments with a scaling factor equal to 3. This fact seems to be more evident in the figures: for Boat, City, and Mountain. When the scaling factor is equal to 5 or 7, the point of the maximum shifts toward the left, as shown in the following Figures 10 and 11.
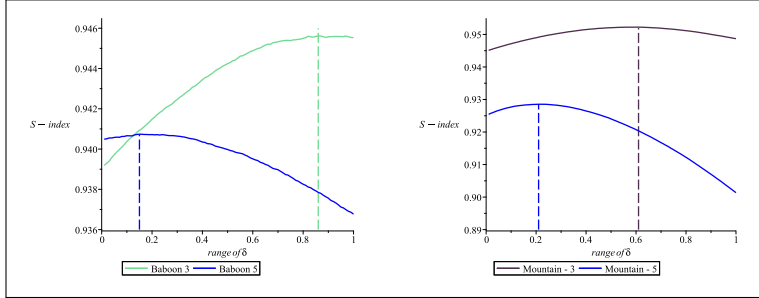
FIGURE 10. $R = 3, 5$: the left shift of the maximum in the plots of the values of the likelihood index S computed for the reconstructed images of the baboon and the mountain with the fuzzy-type algorithm when the parameter δ varies from 0 to 1 with step-size of 0.01.
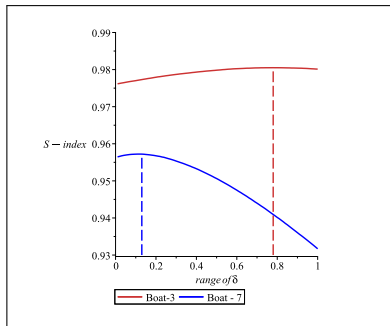
FIGURE 11. $R = 3, 7$: the left shift of the maximum in the plots of the values of the likelihood index S computed for the reconstructed images of the boat with the fuzzy-type algorithm when the parameter δ varies from 0 to 1 with step-size of 0.01.
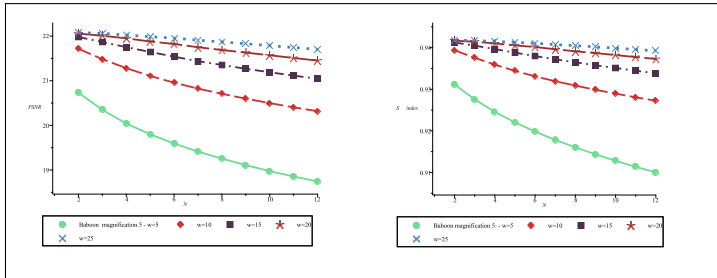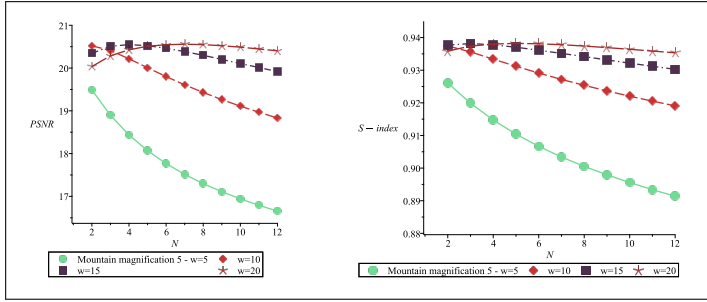
FIGURE 12. The plots of the values of the computed indices for the reconstructed baboon and mountain images when the magnification is 5

Remark 5.3. From the plots of Figure 12 and the data of the subsequent Tables 14 - 17, it seems clear that globally the values of the considered indices are smaller than those achieved in the corresponding cases with magnification factor equal to 3.

This seems quite natural since, we are starting the reconstructions from images that are sensibly smaller than those used in the previous reconstructions, and this can be translated into a process that is based on much less starting information, with respect to the previous case, that can difficulty produce accurate results. Following this reasoning, we can also justify the fact that increasing the value of w the quality of the reconstruction does not improve.

TABLE 4. The numerical values of the PSNR and the likelihood index S, when the images are rescaled by a factor equal to 5. The values must be interpreted as in the previous tables.

	The numerical values of the PSNR and the likelihood index S							
	PSNR index				S index			
Case n=5	$\delta^{\max}$	Fuzzy $\delta^{\max}$	$(N, w)_{\max}$	**SK**	$\delta^{\max}$	Fuzzy $\delta^{\max}$	$(N, w)_{\max}$	**SK**
Baboon	0.30	21.897	(2,25)	22.0775	0.15	0.9407	(2,25)	0.94178
Mountain	0.30	19.05169	$(7, 20)$	20.55734	0.21	0.92854	$(5, 20)$	0.93822

6. APPENDIX

6.1. magnification 3.

We report here the values of the two similarity indices for the rescaled images (magnification 3) using the SK algorithm depending on the values of the two parameters N and w. Each table refers to a single image and a single index of similarity. The values of $(N, w)_{PSNR}$ and $(N, w)_S$ for which the maximum of the similarity indices are reached appear in the tables in bold.

TABLE 5. The numerical values of the PSNR for the baboon image

N	w=5	**w=10**	w=15	w=20	w=25
2	21,85016	**22,43814**	22,32794	22,10527	21,83349
3	21,48853	22,37021	22,41231	22,28217	22,08483
4	21,20701	22,26074	22,43747	22,36078	22,2281
5	20,97893	22,14198	22,42497	22,40758	22,30682
6	20,78909	22,02888	22,39183	22,4312	22,35847
7	20,61677	21,91724	22,35921	22,43585	22,38839
8	20,47379	21,81542	22,29998	22,43023	22,41282
9	20,34389	21,7138	22,24579	22,41857	22,42535
10	20,22084	21,62172	22,19483	22,40215	22,43644
11	20,11594	21,5353	22,13739	22,38263	22,43331
12	20,01313	21,452	22,09212	22,36252	22,43133

TABLE 6. The numerical values of the S-index for the baboon image

N	w=5	w=10	w=15	**w=20**	w=25
2	0,940944	0,947122	0,947393	0,94603	0,944384
3	0,937897	0,945927	0,947648	0,947146	0,945926
4	0,935421	0,944679	0,947305	0,94758	0,946816
5	0,933376	0,943534	0,946765	0,947678	0,947299
6	0,931641	0,942475	0,946223	0,947527	0,947564
7	0,930041	0,94149	0,945736	0,94727	**0,947694**
8	0,928687	0,940611	0,945117	0,946969	0,947649
9	0,927407	0,939758	0,944554	0,946683	0,947556
10	0,926217	0,938982	0,944042	0,94636	0,947444
11	0,925169	0,938254	0,9435	0,946073	0,947228
12	0,924114	0,937539	0,943055	0,945802	0,947034

Danilo Costarelli and Anna Rita Sambucini

TABLE 7. The numerical values of the PSNR for the boat image

N	w=5	w=10	w=15	**w=20**
2	26,1264	28,88491	29,33233	29,1455
3	25,10887	28,2995	29,25153	29,35566
4	24,39938	27,69831	29,01746	**29,3667**
5	23,8721	27,18115	28,73699	29,29081
6	23,45101	26,74578	28,4665	29,16879
7	23,11319	26,36313	28,18154	29,02029
8	22,82393	26,03003	27,90549	28,86864
9	22,57538	25,73335	27,65742	28,70946
10	22,35332	25,46989	27,4174	28,5503
11	22,15799	25,23723	27,20233	28,39299
12	21,98237	25,02072	26,99476	28,23009

TABLE 8. The numerical values of the S-index for the boat image

N	w=5	w=10	w=15	**w=20**
2	0,971368	0,979557	0,980425	0,979874
3	0,967317	0,978083	0,980413	0,98041
4	0,964053	0,976406	0,979877	**0,980565**
5	0,961385	0,974849	0,979184	0,980472
6	0,95908	0,973451	0,978483	0,980232
7	0,957091	0,972149	0,97776	0,979876
8	0,955326	0,970935	0,97699	0,97951
9	0,953716	0,969804	0,976281	0,979102
10	0,952239	0,968759	0,975565	0,978695
11	0,950878	0,96779	0,97491	0,978308
12	0,949631	0,966857	0,974246	0,97789

TABLE 9. The numerical values of the PSNR for the city image

N	w=5	w=10	w=15	**w=20**
2	23,54893	24,94082	25,04948	24,86407
3	22,9495	24,68724	25,06223	25,03318
4	22,51778	24,40862	24,99417	**25,08078**
5	22,18384	24,1397	24,89032	25,07869
6	21,91455	23,89762	24,76533	25,0469
7	21,68927	23,68611	24,64658	25,00216
8	21,49285	23,50061	24,51943	24,94458
9	21,31981	23,32962	24,39139	24,87755
10	21,16648	23,17378	24,26777	24,80927
11	21,02844	23,03034	24,15284	24,74202
12	20,90149	22,90277	24,03818	24,67353

TABLE 10. The numerical values of the S-index for the city image

N	w=5	w=10	w=15	**w=20**
2	0,966276	0,973093	0,974044	0,973677
3	0,963224	0,971649	0,973883	0,974052
4	0,96082	0,970291	0,973345	**0,974093**
5	0,958814	0,969054	0,972696	0,973956
6	0,957099	0,967914	0,972007	0,973693
7	0,955605	0,966908	0,971388	0,973352
8	0,95425	0,965991	0,970786	0,972984
9	0,953023	0,965129	0,970177	0,972603
10	0,951876	0,964339	0,9696	0,972217
11	0,950819	0,963593	0,969084	0,971851
12	0,949828	0,962915	0,968562	0,971497

TABLE 11. The numerical values of the PSNR for the mountain image

N	w=5	w=10	w=15	**w=20**
2	21,76631	23,27749	23,1204	22,68569
3	21,03285	23,07359	23,31022	23,05427
4	20,47727	22,76765	23,33451	23,23154
5	20,04889	22,47274	23,2664	23,31831
6	19,69711	22,19207	23,1556	**23,35247**
7	19,40644	21,93179	23,03366	23,34492
8	19,15224	21,70653	22,89272	23,31629
9	18,93389	21,50075	22,75439	23,26504
10	18,7375	21,30299	22,61814	23,19806
11	18,55898	21,12716	22,4842	23,13559
12	18,40131	20,96599	22,35643	23,06147

TABLE 12. The numerical values of the S-index for the mountain image

N	w=5	w=10	w=15	**w=20**
2	0,943975	0,954693	0,955022	0,953237
3	0,938593	0,952793	0,955499	0,954773
4	0,934135	0,950659	0,95508	0,955388
5	0,930443	0,948655	0,954247	**0,955541**
6	0,927252	0,946779	0,953304	0,955412
7	0,92449	0,945008	0,952377	0,955075
8	0,921978	0,943414	0,951415	0,954651
9	0,919735	0,941943	0,950494	0,954142
10	0,917661	0,940508	0,949581	0,953597
11	0,915726	0,939196	0,948674	0,953094
12	0,913969	0,93795	0,947829	0,952548

TABLE 13. The numerical values of the S-index for the boat image.

[0.01; 0.97616558969266853]	[0.02; 0.97626759036948307]	[0.03; 0.97637292571349765]	[0.04; 0.97646385714780093]
[0.05; 0.97656766410268026]	[0.06; 0.97666971109431622]	[0.07; 0.97676601504799732]	[0.08; 0.97684976768485399]
[0.09; 0.97693415329094790]	[0.10; 0.97701875503287983]	[0.11; 0.97711845540685693]	[0.12; 0.97720917070532198]
[0.13; 0.97730444029463814]	[0.14; 0.97739659135259349]	[0.15; 0.97748522248405789]	[0.16; 0.97758537056798234]
[0.17; 0.97766006093795910]	[0.18; 0.97775185691560795]	[0.19; 0.97785212850572534]	[0.20; 0.97793807337750072]
[0.21; 0.97803451627564830]	[0.22; 0.97809214735277061]	[0.23 ; 0.97817858624931775]	[0.24; 0.97825302960690674]
[0.25; 0.97833929868243896]	[0.26; 0.97840464889659817]	[0.27; 0.97848502055143227]	[0.28; 0.97855926321145992]
[0.29; 0.97862980068570926]	[0.30; 0.97869913397458064]	[0.31; 0.97876408279361438]	[0.32; 0.97883939069455217]
[0.33; 0.97889325483279954]	[0.34; 0.97895463741052202]	[0.35; 0.97901327197545851]	[0.36; 0.97907199917004073]
[0.37; 0.97913480206897852]	[0.38; 0.97920757809296877]	[0.39; 0.97925580726117856]	[0.40; 0.97932396724121917]
[0.41; 0.97938342003468337]	[0.42; 0.97944120549454572]	[0.43; 0.97948467967434194]	[0.44; 0.97954373107267778]
[0.45; 0.97959954043346009]	[0.46; 0.97964355495284927]	[0.47; 0.97968756947223590]	[0.48; 0.97973988978307669]
[0.49; 0.97977845459171642]	[0.50; 0.97983410956975669]	[0.51; 0.97987651850864055]	[0.52; 0.97992034776874026]
[0.53; 0.979998287277874474]	[0.54; 0.98001592612353894]	[0.55; 0.98006724294656333]	[0.56; 0.98011216832412273]
[0.57; 0.98013869127898290]	[0.58; 0.98018823270049082]	[0.59; 0.98021707139646241]	[0.60; 0.98024144843122751]
[0.61; 0.98026273781117690]	[0.62; 0.98028804114238566]	[0.63; 0.98031082803491987]	[0.64; 0.98034139581758906]
[0.65; 0.98037344567456941]	[0.66; 0.98037471161304368]	[0.67; 0.98039501294345210]	[0.68; 0.98042110362663826]
[0.69; 0.98044646871094343]	[0.70; 0.98045438854554323]	[0.71; 0.98046409921993705]	[0.72; 0.98048478650719761]
[0.73; 0.98048520334059863]	[0.74; 0.98049466700260646]	[0.75; 0.98049752308331006]	[0.76; 0.98050144440492548]
[0.77; 0.98050379102258456]	[0.78; 0.98050913266541517]	[0.79; 0.98050024021954696]	[0.80; 0.98050201562106531]
[0.81; 0.98049942199102114]	[0.82; 0.98049304598382936]	[0.83; 0.98048345881562826]	[0.84; 0.98046934823312271]
[0.85; 0.98045710568178235]	[0.86; 0.98045168684758111]	[0.87; 0.98042429934937170]	[0.88; 0.98042289446643149]
[0.89; 0.98040929334697202]	[0.90; 0.98039153933178547]	[0.91; 0.98037545265019832]	[0.92; 0.98036875243925059]
[0.93; 0.98033790676764754]	[0.94; 0.98032297795661794]	[0.95; 0.98029230210603036]	[0.96; 0.98025315064297591]
[0.97; 0.98021506442083295]	[0.98; 0.98019269436169787]	[0.99; 0.98015337307762984]	[1.00; 0.98012437999891566]

In each cell of Table 13, the δ and the corresponding S-index value appear inside the square brackets.

As already mentioned in Section 5, the Boat image was one of those examined in [42] which is the paper that originated the comparison.
If we examine the shapes of the graphs of the [42, Figure 12] and that of Figure 3.(4) we can observe that the qualitative curves are analogous. The maximum in the present paper is obtained for a larger value of the parameter δ, but this may depend both on the floating-point number format and on the fact that in this study we assume that the pixels outside the image have costant value equal to zero, in fact they do not provide additional information (no boundary conditions), while in [42] this is not specified. In any case the difference of the S-index, in Table 13, in the interval between the "$\delta_S^{\max}$" of the two papers is less than $3 \cdot 10^{-4}$ thus we can conclude that the results obtained here confirm those in [42].

6.2. **magnification 5.**

In this subsection, the tables of the two similarity indices are presented for the baboon and the mountain images; as we said before, due to the size of the images, only these two could be taken into consideration for the magnification $R = 5$. In this case the values for which the maximum of the similarity indices is reached are not highlighted.

TABLE 14. The numerical values of the PSNR-index for the baboon image R=5

N	w=5	w=10	w=15	w=20	w=25
2	20,7329147502973	21,7161082496651	21,979365824288	22,0558557949496	22,0775418477414
3	20,3467942537683	21,4828541953169	21,8662212638324	22,0074149690313	22,0615063203985
4	20,0415812414765	21,2811780337	21,7516133283618	21,9493699991135	22,021982797865
5	19,8011752130362	21,1064969190485	21,6437660594206	21,8788040512415	21,9870684510821
6	19,5936090626771	20,9560372953294	21,5387139742664	21,8223810785381	21,9529653869713
7	19,4110677834914	20,8227533041516	21,4372167850169	21,7502537170246	21,9079647824159
8	19,2550258194904	20,7062361523255	21,3526599132005	21,6877191556461	21,8689832613072
9	19,1092740466907	20,5972670626762	21,2666457824789	21,6286366213533	21,8290361881159
10	18,974699199968	20,4979200147237	21,1894189563848	21,5703646320501	21,7851824151841
11	18,8531097177987	20,403559417055	21,113408433493	21,5085279324257	21,7433900697263
12	18,7426431897043	20,3176158516323	21,0436294630194	21,4509224927457	21,7015964927653

TABLE 15. The numerical values of the S-index for the baboon image R=5

N	w=5	w=10	w=15	w=20	w=25
2	0,931130741569984	0,939363412262253	0,941239854957746	0,916674318324023	0,941778411018386
3	0,92756891391697	0,937563742451998	0,940480870856609	0,941408538194208	0,941715991586946
4	0,924526946649478	0,935899284588883	0,939632268132166	0,941022804200496	0,941476867871331
5	0,922040482167492	0,934411108849537	0,938786801456453	0,940544194917489	0,941288343095793
6	0,919811897384866	0,933090651408584	0,937969317984786	0,940145615185713	0,941051511108095
7	0,917812666319892	0,931922835108668	0,937176983211585	0,939616527579889	0,94074592728287
8	0,916027108728919	0,930876540697016	0,936484760763205	0,939115604104002	0,940463622588597
9	0,914360238520628	0,929858832575705	0,935755026347333	0,938689704563101	0,940181438511583
10	0,912790043045284	0,928941839865511	0,935106346729387	0,938211517440502	0,939881885549299
11	0,91133539890389	0,928051202026371	0,934448982668807	0,937729832417396	0,939541986113938
12	0,910025374855824	0,927229798493791	0,933838599030538	0,937278603252143	0,939234834264347

TABLE 16. The numerical values of the PSNR-index for the mountain image R=5

N	$w = 5$	$w = 10$	$w = 15$	$w = 20$
2	19,4878493801042	20,5194643201115	20,3445774937346	20,0352078339142
3	18,8959966960253	20,4106079549201	20,5078456050646	20,2861784442023
4	18,4349923092873	20,2165121177552	20,5479617447969	20,4262893816383
5	18,0690123314328	20,0065933263976	20,5227982717099	20,5094371835843
6	17,7658779676526	19,8011176515348	20,4630175378557	20,54521178183
7	17,5141848124694	19,6066833837114	20,3843693694262	20,557343052487
8	17,2973630657787	19,4295932034864	20,2978171756184	20,5473046959311
9	17,1092673976789	19,2613049769722	20,2016656072662	20,5215375241213
10	16,9415207481794	19,1093674672082	20,1054519195362	20,4886717646383
11	16,7911714644458	18,9661225386627	20,0125175550292	20,4462480907923
12	16,655095783726	18,8313407159141	19,9169980743677	20,402755638215

TABLE 17. The numerical values of the S-index for the mountain image R=5

N	$w = 5$	$w = 10$	$w = 15$	$w = 20$
2	0,926103965141612	0,937437124183007	0,937670007262164	0,935860958605665
3	0,919899927378358	0,935601263616558	0,938177777777779	0,937387596223674
4	0,914731169208424	0,933381859114015	0,937776441539579	0,938012273057373
5	0,910410399419027	0,931204371822803	0,937041626724764	0,938218997821352
6	0,906666129266522	0,929122004357298	0,936115889615106	0,938098634713145
7	0,903401045751634	0,927175061728395	0,935151154684096	0,93781179375454
8	0,900529339143064	0,925371082062454	0,934170806100217	0,937403877995643
9	0,8979444734931	0,9236483805374	0,933156165577341	0,936923384168482
10	0,895572127814088	0,922042527233116	0,932153972403777	0,936412549019608
11	0,893384836601306	0,920517618010166	0,931215003631082	0,935867494553378
12	0,891373623819897	0,919074669571532	0,930259288307916	0,935333710965867

7. CONCLUSIONS

In this article, we compared a construction method of an interval-valued fuzzy set starting from fuzzy sets, introduced in [42] with the SK algorithm and the well-known bicubic method for digital image processing. These algorithms were compared with the use of the PSNR and the likelihood S indices, as well as, by analysing the corresponding processing CPU time. From the numerical results provided in Section 5, it seems to be clear that:

- Based on the analysis of Tables 1 and 2, it seems that the maximum values of the PSNR and likelihood index S are both substantially better in the case of the application of the SK method with sufficiently high w, with respect to other two considered methods. Only when the scaling factor is equal to 3, and we consider the "boat", does the fuzzy-algorithm seem to provide better reconstruction results, at least for the PSNR index. The same consideration can also be applied when the scaling factor is equal to 5. The fuzzy-type algorithm seems to perform substantially better than the bicubic method.
- The CPU analysis given in Table 3, performed only for the best approximations, shows that the bicubic method has the most rapid execution, the mean CPU time employed by the fuzzy-type algorithm is reasonable in term of applicability of the method, while, as we already known, the CPU time is the weak point of the SK algorithm. The higher CPU time seems to be the price to pay to obtain more accurate results.

Author's contribution All authors contributed equally to this work for writing, reviewing and editing. All authors have read and agreed to the published version of the manuscript.

Conflict of interest The authors declare no conflicts of interest.

Data Availability Statement: All the data generated for this study were stored in our laboratory and are not publicly available. Researchers who wish to access the data directly contacted the corresponding author.

REFERENCES

[1] T. Acar, B. R. Draganov: *A characterization of the rate of the simultaneous approximation by generalized sampling operators and their Kantorovich modification*, J. Math. Anal. Appl., **530** (2) (2024), 127740.

[2] T. Acar, M. Turgay: *Approximation by Modified Generalized Sampling Series*, Mediterr. J. Math., **21** (3) (2024), 107.

[3] L. Angeloni, N. Nursel Cetin, D. Costarelli, A. R. Sambucini and G. Vinti: *Multivariate sampling Kantorovich operators: quantitative estimates in Orlicz spaces*, Constr. Math. Anal., **4** (2) (2021), 229–241.

[4] L. Angeloni, D. Costarelli, M. Seracini, G. Vinti and L. Zampogni: *Variation diminishing-type properties for multivariate sampling Kantorovich operators*, Boll. dell'Unione Matem. Ital., **13** (4) (2020), 595–605.

[5] L. Angeloni, G. Vinti: *Multidimensional sampling-Kantorovich operators in BV-spaces*, Open Math., **21** (1) (2023), 20220573,

[6] V. Apollonio, R. D'Autilia, B. Scoppola, E. Scoppola and A. Troiani: *Criticality of Measures on 2-d Ising Configurations: From Square to Hexagonal Graphs*, J. Statistical Phys., **177** (5) (2019), 1009–1021.

[7] K. Atanassov, *Intuitionistic fuzzy sets*, Fuzzy Sets and Systems, **20** (1986), 87–96.

[8] C. Bardaro, P.L. Butzer, R.L. Stens and G. Vinti: *Kantorovich-type generalized sampling series in the setting of Orlicz Spaces*, Sampl. Theory Signal Process. Data Anal., **6** (1) (2007), 29–52

[9] C. Bardaro, I. Mantellini: *Asymptotic formulae for multivariate Kantorovich type generalized sampling series*, Acta Mathematica Sinica (E.S.), **27** (7) (2011), 1247–1258.

[10] C. Bardaro, I. Mantellini: *On convergence properties for a class of Kantorovich discrete operators*, Numer. Funct. Anal. Opt., **33** (2012), 374–396.

[11] G. Biau, L. Devroye: *Lectures on the nearest neighbor method*, Springer International Publishing, Cham, Switzerland (2015).

[12] A Boccuto, A. R. Sambucini: *Some applications of modular convergence in vector lattice setting*, Sampl. Theory Signal Process. Data Anal., **20** (2022), 12.

[13] A Boccuto, A. R. Sambucini: *Abstract integration with respect to measures and applications to modular convergence in vector lattice setting*, Results Math., **78** (2023), 4.

[14] P. Burillo, H. Bustince: *Entropy on intuistionistic fuzzy sets and on interval-valued fuzzy sets*, Fuzzy Sets and Systems, **78** (1996), 305–316.

[15] P. Burillo, H. Bustince: *Construction theorems for intuistionistic fuzzy sets*, Fuzzy Sets and Systems, **84** (1996), 271–281.

[16] H. Bustince, E. Barrenechea, M. Pagola and J. Fernandez: *Interval-valued fuzzy sets constructed from matrices: Application to edge detection*, Fuzzy Sets and Systems, **160** (13) (2009), 1819–1840.

[17] H. Bustince, M. Pagola and E. Barrenechea: *Construction of fuzzy indices from fuzzy DI-subsethood measures: Application to the global comparison of images*, Inf. Sci., **177** (2007), 906–929.

[18] P. L. Butzer, M. Schmidt and E.L. Stark: *Observations on the history of central B-splines*, Arch. Hist. Exact Sci., **39.2** (1988), 137–156.

[19] D. Candeloro, A. R. Sambucini: *Filter Convergence and Decompositions for Vector Lattice-Valued Measures*, Mediterr. J. Math., **12** (2015), 621–637.

[20] M. Cantarini, D. Costarelli and G. Vinti: *Approximation of differentiable and not differentiable signals by the first derivative of sampling Kantorovich operators*, J. Math. Anal. Appl., **509** (1) (2022), 125913.

[21] M. Cantarini, D. Costarelli and G. Vinti: *Approximation results in Sobolev and fractional Sobolov spaces by sampling Kantorovich operators*, Fract. Calc. Appl. Anal., **26** (2023), 2493-2521.

[22] M. Castro, D.M. Ballesteros and D. Renza: *A dataset of 1050-tampered color and grayscale images (CG-1050)*, Data in brief, (2019).

[23] N. Çetin, D. Costarelli, M. Natale and G. Vinti, *Nonlinear multivariate sampling Kantorovich operators: quantitative estimates in functional spaces*, Dolomites Res. Notes Approx., **15** (2022), 12–25.

[24] F. Cluni, D. Costarelli, V. Gusella and G. Vinti, *Reliability increase of masonry characteristics estimation by sampling algorithm applied to thermographic digital images*, Probabilistic Eng. Mech., **60** (2020), 103022.

[25] D. Costarelli, A. Croitoru, A. Gavriluţ, A. Iosif and A. R. Sambucini: *The Riemann-Lebesgue integral of interval-valued multifunctions*, Mathematics, **8** (12) (2020), 1–17, 2250.

[26] D. Costarelli, M. Natale and G. Vinti: *Convergence results for nonlinear sampling Kantorovich operators in modular spaces*, Numer. Funct. Anal. Optim., **44** (12) (2023), 1276–1299.

[27] D. Costarelli, M. Piconi and G. Vinti: *The multivariate Durrmeyer-sampling type operators: approximation in Orlicz spaces*, Dolomites Res. Notes Approx., **15** (2022), 128–144.

[28] D. Costarelli, M. Piconi and G. Vinti: *Quantitative estimates for Durrmeyer-sampling series in Orlicz spaces*, Sampl. Theory Signal Process. Data Anal., **21** (2023), 3.

[29] D. Costarelli, A. R. Sambucini: *Approximation results in Orlicz spaces for sequences of Kantorovich max-product neural network operators*, Results Math., **73** (2018), 15.

[30] D. Costarelli, A. R. Sambucini and G. Vinti: *Convergence in Orlicz spaces by means of the multivariate max-product neural network operators of the Kantorovich type*, Neural Comput. Appl., **31** (9) (2019), 5069–5078.

[31] D. Costarelli, M. Seracini and G. Vinti: *A comparison between the sampling Kantorovich algorithm for digital image processing with some interpolation and quasi-interpolation methods*, Appl. Math. Comput., **374** (2020), 125046.

[32] D. Costarelli, M. Seracini and G. Vinti: *A segmentation procedure of the pervious area of the aorta artery from CT images without contrast medium*, Math. Methods Appl. Sci., **43** (2020) 114-133.

[33] D. Costarelli, G. Vinti: *Approximation properties of the sampling Kantorovich operators: regularization, saturation, inverse results and Favard classes in L^p-spaces*, J. Fourier Anal. Appl., **28** (2022), 49.

[34] I. Couso, H. Bustince: *From Fuzzy Sets to Interval-Valued and Atanassov Intuitionistic Fuzzy Sets: A Unified View of Different Axiomatic Measures*, in IEEE Trans. Fuzzy Syst., **27** (2) (2019), 362–371.

[35] A. Croitoru, A. Gavriluţ, A. Iosif and A. R. Sambucini: *A note on convergence results for varying interval valued multisubmeasures*, Math. Found. Comput., **4** (4) (2021), 299–310.

[36] R. D'Autilia, L.N. Andrianaivo and A. Troiani: *Parallel simulation of two-dimensional Ising models using probabilistic cellular automata*, J. Stat. Phys., **184** (2021), 1–22.

[37] L. Di Piazza, V. Marraffa, K. Musiał and A. R. Sambucini: *Convergence for varying measures*, J. Math. Anal. Appl., **518** (2023), 126782.

[38] L. Di Piazza, V. Marraffa, K. Musiał and A. R. Sambucini: *Convergence for varying measures in the topological case*, Ann. Mat. Pura Appl., (4), **203** (2024), 71–86.

[39] L. Di Piazza, V. Marraffa and B. Satco: *Measure differential inclusions: existence results and minimum problems*, Set-Valued Var. Anal., **29** (2) (2021), 361–382.

[40] B. R. Draganov: *A fast converging sampling operator*, Constr. Math. Anal., **5** (4) (2022), 190-201.

[41] R.C. Gonzalez, R.E. Woods: *Digital Image Processing*, Pearson Prenctice Hall (2007).

[42] A. Jurio, D. Paternain, C. Lopez-Molina, H. Bustince, R. Mesiar and G. Beliakov: *A construction method of interval-valued Fuzzy Sets for image processing*, 2011 IEEE Symposium on Advances in Type-2 Fuzzy Logic Systems (T2FUZZ), (2011), 16–22.

[43] Y. Kolomoitsev, M. Skopina: *Approximation by sampling-type operators in L^p-spaces*, Math. Methods Appl. Sci., **43** (16) (2020), 9358–9374.

[44] Y. Kolomoitsev, M. Skopina: *Quasi-projection operators in weighted L^p spaces*, Appl. Comput. Harmon. Anal., **52** (2021), 165–197.

[45] D. La Torre, F. Mendevil: *The Monge-Kantorovich metric on multimeasures and self-similar multimeasures*, Set-Valued Var. Anal., **23** (2015), 319–331.

[46] J. Liu, Z. Gan and X. Zhu: *Directional Bicubic Interpolation - A New Method of Image Super-Resolution*, Proc. 3rd International Conf. Multimedia Technology (ICMT-13), In: Advances in Intelligent Systems Research, (2013).

[47] A. Osowska-Kurczab, T. Les, T. Markiewicz, M. Dziekiewicz, M. Lorent, S. Cierniak, D. Costarelli, M. Seracini and G. Vinti: *Improvement of renal image recognition through resolution enhancement*, Expert Syst. Appl., **213** (A) (2023), 118836.

[48] E. Pap, A. Iosif and A. Gavriluţ: *Integrability of an Interval-valued Multifunction with respect to an Interval-valued Set Multifunction*, Iran. J. Fuzzy Syst., **15** (3) (2018), 47–63.

[49] B. Scoppola, A. Troiani and M. Veglianti: *Shaken dynamics on the 3d cubic lattice*, Electron. J. Probab., **27** (2022), 1–26.

[50] A. Tanchenko: *Visual-PSNR measure of image quality*, J. Vis. Commun. Image Represent., **25** (5) (2014), 874–878.

[51] The Vision and Image Processing Lab at University of Waterloo, Greyscale Set 2, `https://links.uwaterloo.ca/Repository.html`

[52] G. Vinti, L. Zampogni: *Approximation results for a general class of Kantorovich type operators*, Adv. Nonlinear Stud., **14** (4) (2014), 991–1011.

DANILO COSTARELLI
UNIVERSITY OF PERUGIA
DEPARTMENT OF MATHEMATICS AND COMPUTER SCIENCES
1 VIA VANVITELLI, 06124, PERUGIA, ITALY
ORCID: 0000-0001-8834-8877
Email address: `danilo.costarelli@unipg.it`

ANNA RITA SAMBUCINI
UNIVERSITY OF PERUGIA
DEPARTMENT OF MATHEMATICS AND COMPUTER SCIENCES
1 VIA VANVITELLI, 06124, PERUGIA, ITALY
ORCID: 0000-0003-0161-8729
Email address: `anna.sambucini@unipg.it`